Inorg. Chem. **2007**, *46*, 6261–6270

Electronic and Magnetic Interactions in π-Stacked Bisthiadiazinyl Radicals

Alicea A. Leitch,[†] Richard T. Oakley,*[,†] Robert W. Reed,[†] and Laurence K. Thompson[‡]

Department of Chemistry, University of Waterloo, Waterloo, Ontario N2L 3G1 Canada, and Department of Chemistry, Memorial University of Newfoundland, St. John's, Newfoundland A1B 3X7, Canada

Received January 10, 2007

The preparation of two bisthiadiazinyls (**7**, R_1 = Me, Et; R_2 = Cl, R_3 = Ph), the first examples of a new class of resonance-stabilized heterocyclic thiazyl radical, are reported. Both radicals have been characterized in solution by EPR spectroscopy and cyclic voltammetry, which confirm highly delocalized spin distributions and low electrochemical cell potentials, features which augur well for the use of these materials as building blocks for neutral radical conductors. In the solid state, the radicals are undimerized, crystallizing in slipped π-stack arrays which ensure the availability of electrons as potential charge carriers. However, despite these favorable electrochemical and structural properties, both materials exhibit low conductivities, with σ(300K) < 10^{-7} S cm^{-1}, a result which can be rationalized in terms of their EHT band electronic structures, which indicate that intermolecular interactions lateral to the π-stacks are limited. The materials are thus very 1-D with low bandwidths, so that a Mott insulating state prevails. When R_1 = Me, the intermolecular overlap along the π-stacks is weak and the material is essentially paramagnetic. When R_1 = Et, intermolecular π-overlap is greater and variable-temperature magnetic susceptibility measurements indicate a strongly antiferromagnetically coupled system, the behavior of which has been modeled in terms of a molecular-field modified 1-D Heisenberg chain of $S = {}^1/_2$ centers. Broken-symmetry DFT methods have been used to estimate the magnitude of individual exchange interactions within both structures.

Introduction

Heterocyclic thiazyl radicals represent versatile building blocks for the design of new molecular materials,[1] with potential applications as organic ferromagnets,[2,3] magneto-thermal switches,[4–6] and as spin-bearing ligands[7] for coupling magnetic metal centers. Their use in the development of single-component conductors has also been actively explored.[8] In an ideal neutral radical conductor, the unpaired electrons serve as charge carriers, with orbital overlap between radical SOMOs (singly occupied molecular orbitals) affording a $^1/_2$-filled energy band and a metallic ground state.[9] To date, however, no such system has ever been generated. Most radicals dimerize, and even when association

* To whom correspondence should be addressed. E-mail: oakley@uwaterloo.ca.
[†] University of Waterloo.
[‡] Memorial University.

(1) (a) Rawson, J. M.; Alberola, A.; Whalley, A. *J. Mater. Chem*. **2006**, *16*, 2560. (b) Hicks, R. G. *Org. Biomol. Chem*. **2007**, *5*, 1321. (c) Breher, F. *Coord. Chem. Rev*. **2007**, *251*, 1007.
(2) (a) Banister, A. J.; Bricklebank, N.; Lavender, I.; Rawson, J. M.; Gregory, C. I.; Tanner, B. K.; Clegg, W.; Elsegood, M. R. J.; Palacio, F. *Angew. Chem., Int. Ed. Engl*. **1996**, *35*, 2533. (b) Alberola, A.; Less, R. J.; Pask, C. M.; Rawson, J. M.; Palacio, F.; Oliete, P.; Paulsen, C.; Yamaguchi, A.; Murphy, D. M.; Farley, R. D. *Angew. Chem., Int. Ed.* **2003**, *42*, 4782.
(3) (a) Mito, M.; Fujino, M.; Deguchi, H.; Takagi, S.; Fujita, W.; Awaga, K. *Polyhedron* **2005**, 2501. (b) Fujita, W.; Awaga, K.; Takahashi, M.; Takeda, M.; Yamazaki, T. *Chem. Phys. Lett*. **2002**, *362*, 97. (c) Awaga, K.; Tanaka, T.; Shirai, T.; Fujimori, M.; Suzuki, Y.; Yoshikawa, H.; Fujita, W. *Bull. Chem. Soc. Jpn*. **2006**, *79*, 25.
(4) Barclay, T. M.; Cordes, A. W.; George, N. A.; Haddon, R. C.; Itkis, M. E.; Mashuta, M. S.; Oakley, R. T.; Patenaude, G. W.; Reed, R. W.; Richardson, J. F.; Zhang, H. *J. Am. Chem. Soc*. **1998**, *120*, 352.
(5) (a) Fujita, W.; Awaga, K. *Science* **1999**, *286*, 261. (b) McManus, G. D.; Rawson, J. M.; Feeder, N.; van Duijn, J.; McInnes, E. J. L.; Novoa, J. J.; Burriel, R.; Palacio, F.; Oliete, P. *J. Mater. Chem.* **2001**, *11*, 1992.
(6) (a) Brusso, J. L.; Clements, O. P.; Haddon, R. C.; Itkis, M. E.; Leitch, A. A.; Oakley, R. T.; Reed, R. W.; Richardson, J. F. *J. Am. Chem. Soc*. **2004**, *126*, 8256. (b) Brusso, J. L.; Clements. O. P.; Haddon, R. C.; Itkis, M. E.; Leitch, A. A.; Oakley, R. T.; Reed, R. W.; Richardson, J. F. *J. Am. Chem. Soc*. **2004**, *126*, 14692.
(7) (a) Hearns, N. G. R.; Preuss, K. E.; Richardson, J. F.; Bin-Salamon, S. *J. Am. Chem. Soc.* **2004**, *126*, 9942. (b) Jennings, M.; Preuss, K. E.; Wu, J. *Chem. Commun*. **2006**, 341.
(8) (a) Cordes, A. W.; Haddon, R. C.; Oakley, R. T. *Adv. Mater*. **1994**, *6*, 798. (b) Cordes, A. W.; Haddon, R. C.; Oakley, R. T. *Phosphorus, Sulfur, Silicon Relat. Elem.* **2004**, *179*, 673.

10.1021/ic0700405 CCC: $37.00
Published on Web 07/11/2007

Chart 1

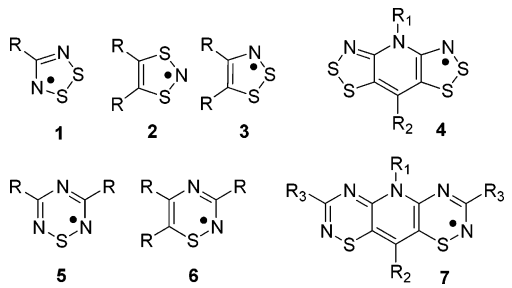

is overcome, typically by the use of steric bulk, the resulting low bandwidth, *W*, coupled with the high on-site Coulomb repulsion energy, *U*, leads to a Mott insulating state.[10] Insofar as *U* reaches a maximum for systems with a half-filled band ($f = {}^1/_2$), the need to control this parameter is critical. To this end, we have sought radicals with good ion energetics, that is, low gas-phase disproportionation enthalpies ΔH_{disp} (= IP − EA) and correspondingly small solution cell potentials E_{cell},[11] as these molecular observables serve as guides to the value of the more elusive *U*.[12−14]

Within the thiazyl radical family, the most actively studied systems, from a materials perspective, have been 1,2,3,5-dithiadiazolyls, **1**, and 1,3,2- and 1,2,3- dithiazolyls, **2** and **3** (Chart 1). Attempts to suppress dimerization have met with some success, and in dithiazolyls, substituent effects can be used to modify redox properties and, hence, lower the on-site Coulomb repulsion, *U*.[4,6,13] Dramatic improvements in stability, structure, and redox properties can be achieved by use of resonance effects, as in the bisdithiazolyls **4**.[8b,15−17] In the solid state, these latter radicals adopt undimerized π-stacked structures, but the loss in intermolecular overlap and hence bandwidth occasioned by slippage of the radicals along the π-stacks leads to Mott insulating ground states. Replacement of sulfur by selenium, however, leads to a marked increase in conductivity and decrease in activation energy.[18]

Six-membered ring systems, such as thiatriazinyls **5** and thiadiazinyls **6** have also been pursued, although less extensively, as the former exhibit a tendency to dimerize quite strongly at sulfur[19] and the latter are thermally unstable and have only been isolated as condensed ring variants.[20] In order to explore the effects of resonance stabilization of the type found in **4**, we have pursued the preparation and characterization of resonance-stabilized bisthiadiazinyls **7**. Herein we describe the synthesis of the first two examples of this ring system, with R_1 = Me, Et; R_2 = Cl, R_3 = Ph.[21] The spin distributions and ion energetics of these radicals have been examined by EPR spectroscopy and cyclic voltammetry, and the derived hyperfine coupling constants and cell potentials cross-matched with the results of DFT (density functional theory) calculations. The crystal structures, EHT (extended Hückel theory) band structures, electrical conductivities, and magnetic properties of both radicals are compared with those found for **4**. The results indicate that while the basic framework of **7** has many of the desired attributes for an effective building block for a molecular conductor, the presence of the R_3 ligands, which are not found in **4**, leads to a reduction in bandwidth, *W*, and loss in conductivity relative to **4**. The magnetic interactions within these systems are also simplified relative to those found in **4** and, in the case of **7** (R_1 = Et), we have been able to model the temperature dependence of the magnetic susceptibility in terms of an antiferromagnetic 1-D Heisenberg chain of $S = {}^1/_2$ centers.

Results and Discussion

Synthesis. The monofunctional benzothiadiazine framework can be assembled by a variety of synthetic pathways.[22] Of these, the favored route has involved the cyclocondensation of an amidine with a sulfur halide.[22a] The amidine can be prepared from the reaction of an arylamine with $AlCl_3$ and the appropriate nitrile[23,24] or by reaction of the amine

(9) (a) Haddon, R. C. *Nature*, **1975**, *256*, 394. (b) Haddon, R. C. *Aust. J. Chem*. **1975**, *28*, 2333. (c) Haddon, R. C. *Aust. J. Chem*. **1975**, *28*, 2334.

(10) Mott, N. F. *Metal-insulator Transitions*; Taylor and Frances: London, 1990.

(11) ΔH_{disp} is the enthalpy change for the conversion of two gas-phase radicals, R, into a cation/anion pair, i.e., 2 R $\rightleftarrows$ $R^+ + R^-$, and accordingly is equal to the difference between the ionization potential (IP) and electron affinity (EA). The solution-based cell potential $E_{\text{cell}} = E_{1/2}(\text{ox}) - E_{1/2}(\text{red})$ is the difference between the half-wave potentials for the oxidation and reduction processes.

(12) Kaszynski, P. *J. Phys. Chem. A* **2001**, *105*, 7626.

(13) Cordes, A. W.; Mingie, J. R.; Oakley, R. T.; Reed, R. W.; Zhang, H. *Can. J. Chem*. **2001**, *79*, 1352.

(14) Boeré, R. T.; Roemmele, T. L. *Coord. Chem. Rev.* **2000**, *210*, 369.

(15) Beer, L.; Brusso, J. L.; Cordes, A. W.; Haddon, R. C.; Itkis, M. E.; Kirschbaum, K.; MacGregor, D. S.; Oakley, R. T.; Pinkerton, A. A.; Reed, R. W. *J. Am. Chem. Soc.* **2002**, *124*, 9498.

(16) (a) Beer, L.; Brusso, J. L.; Cordes, A. W.; Haddon, R. C.; Godde, E.; Itkis, M. E.; Oakley, R. T.; Reed, R. W. *Chem. Commun.* **2002**, 2562. (b) Beer, L.; Britten, J. F.; Brusso, J. L.; Cordes, A. W.; Haddon, R. C.; Itkis, M. E.; MacGregor, D. S.; Oakley, R. T.; Reed, R. W.; Robertson, C. M. *J. Am. Chem. Soc*. **2003**, *125*, 14394.

(17) Beer, L.; Britten, J. F.; Clements, O. P.; Haddon, R. C.; Itkis, M. E.; Matkovich, K. M.; Oakley, R. T.; Reed, R. W. *Chem. Mater*. **2004**, *16*, 1564.

(18) (a) Beer, L.; Brusso, J. L.; Haddon, R. C.; Itkis, M. E.; Kleinke, H.; Leitch, A. A.; Oakley, R. T.; Reed, R. W.; Richardson, J. F.; Secco, R. A.; Yu, X. *J. Am. Chem. Soc*. **2005**, *127*, 1815. (b) Beer, L.; Brusso, J. L.; Haddon, R. C.; Itkis, M. E.; Oakley, R. T.; Reed, R. W.; Richardson, J. F.; Secco, R. A.; Yu, X. *Chem. Commun*. **2005**, 5745. (c) Brusso, J. L.; Cvrkalj, K.; Leitch, A. A.; Oakley, R. T.; Reed, R. W.; Robertson, C. M. *J. Am. Chem. Soc*. **2006**, *128*, 15080. (d) Brusso, J. L.; Derakhshan, S.; Itkis, M. I.; Kleinke, H.; Haddon, R. C.; Oakley, R. T.; Reed, R. W.; Richardson, J. F.; Robertson, C. M.; Thompson, L. K. *Inorg. Chem*. **2007**, *46*, 10958.

(19) Hayes, P. J.; Oakley, R. T.; Cordes, A. W.; Pennington, W. T. *J. Am. Chem. Soc*. **1985**, *107*, 1346.

(20) Zienkiewicz, J.; Kaszynski, P.; Young, V. G., Jr. *J. Org. Chem*. **2004**, *69*, 7525.

(21) A preliminary communication on part of this work has been published. See Beer, L.; Haddon, R. C.; Itkis, M. E.; Leitch, A. A.; Oakley, R. T.; Reed, R. W.; Richardson, J. F.; VanderVeer, D. G. *Chem. Commun*. **2005**, 1218.

(22) (a) Zienkiewicz, J.; Kaszynski, P.; Young, V. G.; Jr. *J. Org. Chem*. **2004**, *69*, 2551. (b) Gilchrist, T. L.; Rees, C. W.; Vaughan, D. *J. Chem Soc., Perkin Trans*. **1983**, *1*, 55. (c) Levchenko, E. S.; Borovikova, G. S.; Borovik, E. I.; Kalinin,V. N. *Russ. J. Org. Chem.* **1984**, *20*, 176. (d) Shermolovich, Y. G.; Simonov, Y. A.; Dvorkin, A. A.; Polumbrik, O. M.; Borovikova, G. S.; Kaminskaya, E. I.; Levchenko, E. S.; Markovskii, L. N. *Russ. J. Org. Chem*. **1989**, *25*, 550. (e) Gilchrist, T. L.; Rees, C. W.; Vaughan, D. *J. Chem. Soc., Perkin Trans*. **1983**, *1*, 49. (f) Gilchrist, T. L.; Rees, C. W.; Vaughan, D. *J. Chem. Soc., Chem. Commun*. **1978**, 1049. (g) Markovskii, L. N.; Darmokhval, E. A.; Levchenko, E. S. *Russ. J. Org. Chem*. **1973**, *9*, 2055.

(23) Oxley, P.; Partridge, M. W.; Short, W. F. *J. Chem. Soc*. **1947**, 1110.

(24) Finch, N.; Ricca, S., Jr.; Werner, L. H.; Rodebaugh, R. *J. Org. Chem*. **1980**, *45*, 3416.

Scheme 1

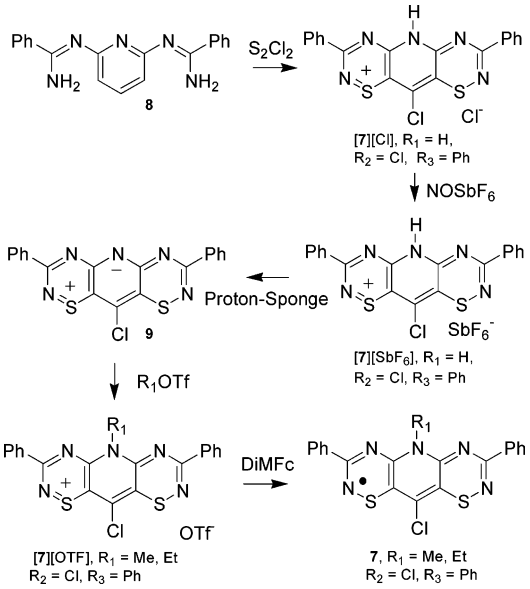

with an orthoester.[25] Alternatively, the thiadiazine skeleton can be constructed in a single step by the condensation of an aminothiol with hydroximoyl chloride.[26] Generation of the thiadiazinyl radicals can then be achieved by oxidation of corresponding thiadiazines, although in principle, they should be accessible by reduction of the corresponding thiadiazinum cations. In our work on bifunctional materials, we have focused on the bisamidine route (Scheme 1).

The preparation of the pyridine-bridged bisamidine **8** could not be achieved by the condensation of ethyl orthobenzoate with diaminopyridine, as this reaction led to polymeric products. The condensation of diaminopyridine with benzonitrile in the presence of $AlCl_3$ was, however, more successful, affording **8** in good yield. Treatment of **8** with sulfur monochloride at reflux in chlorobenzene then furnished the bisthiadiazine framework as the protonated salt [**7**][Cl] (R_1 = H, R_2 = Cl, R_3 = Ph). Metathesis of the crude chloride to the crystalline SbF_6^- salt, followed by deprotonation of the latter with Proton-Sponge, yielded the zwitterion **9**, which was in turn alkylated with methyl or ethyl triflate (trifluoromethanesulfonate) to afford the bisthiadiazinium triflates [**7**][OTf] (R_1 = Me, Et; R_2 = Cl, R_3 = Ph). These salts are highly colored, as expected from their antiaromatic (16π-electron) count. In the solid state the salts have an iridescent red/green hue, while in solution they are deep blue with a strong (red) fluorescence (Figure 1), as found in other heterocyclic zwitterionic dyes.[27]

The choice of reagent for the chemical reduction of these bisthiadiazinium triflates [**7**][OTf] to the respective radicals **7** was made on the basis of an analysis of the relevant half-wave potentials (vide infra). From these measurements, it was apparent that bisthiadiazinyls **7** are significantly less

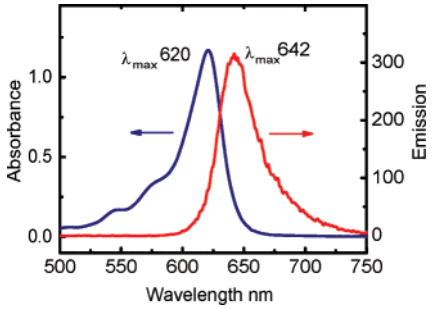

Figure 1. Absorption and fluorescence (λ_{ex} = 620 nm) spectra of [**7**][OTf] (R_1 = Me, R_2 = Cl, R_3 = Ph) in MeCN.

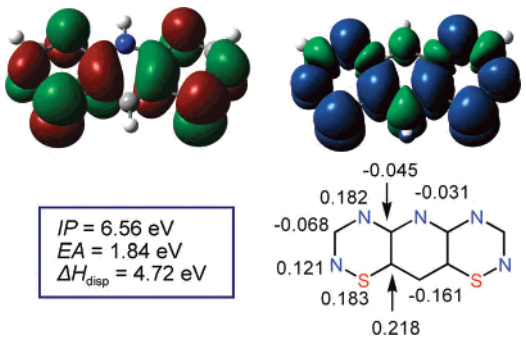

Figure 2. B3LYP/6-31G(d,p) SOMO (left) and spin density (right) of **7** (R_1 = R_2 = R_3 = H). Ion energetics data and spin densities are shown below.

electron-rich than bisdithiazolyls **4**, and reduction of cations $[\mathbf{7}]^+$ could be easily effected with dimethylferrocene (DiMFc). The radicals so obtained are sparingly soluble in organic media, are relatively stable to aerial oxidation, and are extremely thermally stable (in contrast to **4**). Accordingly, single crystals of **7** (R_1 = Me, Et) suitable for X-ray work were grown by vacuum sublimation at 200 °C.

Ion Energetics, EPR Spectra, and Electrochemistry. We have explored the electronic structure of bisthiadiazinyls by means of DFT calculations at the B3LYP/6-31G(d,p) level on a model radical with R_1 = R_2 = R_3 = H. The extent of spin delocalization can be related to the distribution of the a_2 SOMO (Figure 2), which may be considered as an out-of-phase combination of the SOMOs of two monofunctional thiadiazines. The resultant total spin densities illustrated in Figure 2 confirm this simple one-electron molecular orbital picture. There is heavy spin density in the two thiadiazine rings, with relatively low negative spin concentrations along the central axis of the molecule, that is, along the nodal plane of the SOMO. Also provided in Figure 2 are the ΔSCF values of the IP and EA, which are both higher than those found for **4** (IP = 6.16 eV, EA = 1.39 eV for R_1 = R_2 = H).[16] The consequent disproportionation energy, ΔH_{disp}, is, however, almost the same as that of **4** ΔH_{disp} = 4.77 eV for R_1 = R_2 = H).[16]

The EPR spectra of **7** (R_1 = Me, Et; R_2 = Cl, R_3 = Ph) are well explained in terms of the above electronic summary. The X-band spectra of both radicals, obtained at ambient temperature on samples dissolved in CH_2Cl_2, have *g* values slightly larger than the free-electron value (an effect attributable to spin−orbit coupling on sulfur) and display a complex hyperfine multiplet pattern dominated by coupling to the four

(25) Benko, V. P.; Pallos, L. *J. Prakt. Chem.* **1971**, *313*, 179.
(26) Abdelhamid, A. O.; Khalifa, F. A.; Ghabrial, S. S. *Phosphorus, Sulfur, Silicon Relat. Elem.* **1988**, *40*, 41.
(27) (a) Hutchison, K.; Srdanov, G.; Hicks, R.; Yu, H.; Wudl, F.; Strassner, T.; Nendel, M.; Houk, K. N. *J. Am. Chem. Soc.* **1998**, *120*, 2989. (b) Langer, P.; Bodtke, A.; Saleh, N. N. R.; Görls, H.; Schreiner, P. R. *Angew. Chem., Int. Ed.* **2005**, *44*, 5255. (c) Prieto, J. B.; Arbeloa, F. L.; Martínez, V. M.; Arbeloa, I. L. *Chem. Phys.* **2004**, *296*, 13.

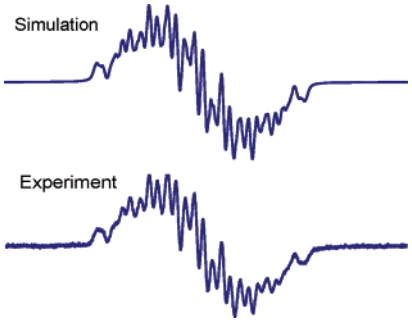

Figure 3. EPR spectrum of **7** (R_1 = Et, R_2 = Cl, R_3 = Ph), in CH_2Cl_2. SW = 4 T, L/G = 0.10, LW = 0.032 mT.

Table 1. Electrochemical Potentials[a] and EPR Data[b]

	7[c]		**4**[c]	
	R_1 = Me	R_1 = Et	R_1 = Me	R_1 = Et
$E_{1/2}^{(+1/+2)}$	1.88[d]	1.88[d]	1.415	1.39
$E_{1/2}^{(0/+1)}$	0.355	0.339	0.005	−0.018
$E_{1/2}^{(-1/0)}$	−0.476	−0.486	−0.835	−0.845
E_{cell}	0.831	0.825	0.84	0.827
g	2.0059	2.0059	2.008274	2.008208
a_N (NR_1)[e]	0.069	0.070	0.060	0.060
	(−0.097)	(0.097)	(−0.069)	(−0.069)
a_N (C*N*C)[e]	0.268	0.271	−	−
	(0.327)	(0.327)		
a_N (C*N*S)[e]	0.184	0.187	0.310	0.310
	(0.238)	(0.238)	(0.357)[f]	(0.357)[f]

[a] $E_{1/2}$ values (V) in MeCN, reference SCE; $E_{cell} = E_{1/2}^{0/+1} - E_{1/2}^{-1/0}$. [b] Coupling constants, a_N, in mT. [c] R_2 = Cl for both **7** and **4**; R_3 = Ph for **7**. [d] Irreversible wave, E_{pa} value cited. [e] B3LYP/6-31G(d,p) values (in parenthesis) from a model with all R = H. [f] Coupling only possible to the C*N*S nitrogens of **4**.

^{14}N nuclei (I = 1) within the thiadiazine rings. Smaller couplings to ^{35}Cl and ^{37}Cl, to the pyridine nitrogen, and to the alkyl and aryl protons lead to a general line broadening. In the case of the methyl radical, the appearance of the spectrum was sharpened by deuteration of the phenyl rings,[21] but the spectrum of the ethyl derivative (Figure 3) was reasonably well resolved without such measures. Hyperfine couplings were extracted by spectral simulation with Simfonia and WinSim, and assignments were confirmed by comparison of the experimental coupling constants with values predicted from B3LYP/6-31G(d,p) calculations on a model **7** with $R_1 = R_2 = R_3$ = H. The derived experimental and computed a_N values listed in Table 1[28] are consistent with a highly delocalized spin distribution, with approximately equal spin densities on the two chemically distinct nitrogens within the thiadiazine rings. The a_N coupling constants and the calculated spin densities on these nitrogens are about one-half the values of those found in monofunctional thiadiazinyls and thiatriazinyls, as would be expected given that the unpaired spin distribution is delocalized over two rings rather than one. A similar effect has been noted in bisdithiazolyls **4**.[15,16] The discrepancy between the observed a_N values for **7** (R_1 = Me, Et; R_2 = Cl, R_3 = Ph) and those calculated for the model with $R_1 = R_2 = R_3$ = H simply reflect the effects of spin delocalization onto the ligands, particularly the phenyl groups.

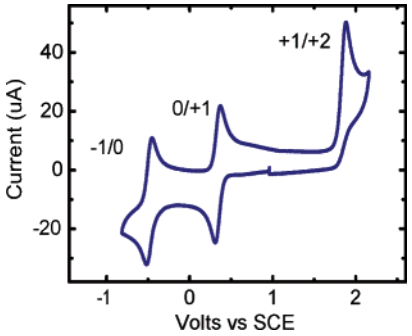

Figure 4. Cyclic voltammetry of [**7**][OTf] (R_1 = Et, R_2 = Cl, R_3 = Ph) in MeCN.

The electrochemical behavior of **7** (R_1 = Me, Et; R_2 = Cl, R_3 = Ph) has been probed by cyclic voltammetry on solutions of the salts [**7**][OTf] in MeCN (with 0.1 M *n*-Bu_4NPF_6 supporting electrolyte). The results, presented in the form of half-wave potentials, $E_{1/2}$, are summarized in Table 1. A representative scan (for R_1 = Et) is shown in Figure 4. Both systems (R_1 = Me, Et) show three waves, corresponding to the −1/0, 0/+1, and +1/+2 processes. Within this group, the +1/+2 wave is strongly irreversible, a feature in sharp contrast to the behavior of bisdithiazolyls **4**, where the +1/+2 wave is invariably reversible.[15,16] Nonetheless, the two more pertinent couples, corresponding to electron transfer to/from the radical, are clearly reversible. In accord with the DFT estimates of the IP and EA values (vide supra), which are higher than those found for **4**, the half-wave potentials $E_{1/2}^{(-1/0)}$ and $E_{1/2}^{(0/+1)}$ of **7** are shifted anodically by some 300 mV from those found for **4**, thereby providing experimental confirmation that the bisthiadiazinyl framework is more electronegative. Nonetheless, and as predicted by the computed ΔH_{disp} values, the cell potentials, E_{cell}, for **7** (R_1 = Me, Et) are considerably smaller (by 300 mV) than those found for monofunctional benzo-fused thiadiazinyls **6**[20] and comparable to those found for bisdithiazolyls **4**. The effect of resonance stabilization, to lower the energetics of charge transfer in solution, is thus clearly established. This conclusion augurs well for a lowered value for U in the solid state.

Crystal Structures. Single-crystal X-ray structure determinations of **7** (R_1 = Me, Et; R_2 = Cl, R_3 = Ph) have confirmed that both radicals preserve their S = 1/2 identity in the solid state, that is, they do *not* dimerize. Crystal data for the two radicals, as well as the triflate salt [**7**][OTf] (R_1 = Me, R_2 = Cl, R_3 = Ph), are summarized in Table 2. Crystals of the methyl-substituted radical, grown by vacuum sublimation, are extremely fibrous needles and are poor X-ray diffractors, as a result of which X-ray data collection was performed at 173 K, and the refinement was less than ideal, although clearly sufficient to establish the molecular framework and the packing pattern. Needles of the ethyl derivative are thicker and more robust; as a result of which, it was possible to collect good X-ray data at ambient temperature. ORTEP drawings of the two radicals are provided in

(28) Smaller hyperfine couplings to other nuclei were also obtained from the simulations. For R_1 = Me, a_H (CH_3) 0.033, a_{Cl} 0.029/0.024 (^{35}Cl/^{37}Cl) mT. For R_1 = Et, a_H (CH_2) 0.022, a_{Cl} 0.027/0.023 (^{35}Cl/^{37}Cl) mT.

Table 2. Crystallographic Data

	7 (R_1 = Et)[a]	**7** (R_1 = Me)[a,b]	[**7**][OTf] (R_1 = Me)[a,b]
a, Å	5.6870(2)	3.9232(8)	8.4474(6)
b, Å	25.3004(8)	27.527(6)	13.9712(10)
c, Å	13.5877(4)	16.378(3)	40.105(3)
β, deg	91.742(2)	90.17(3)	-
V, Å^3	1954.14(11)	1768.7(6)	4733.2(6)
ρ(calcd), g cm^{-1}	1.485	1.588	1.605
space group	$P2_1/n$	$P2_1/c$	*Pbca*
Z	4	4	8
temp, K	298(2)	173(2)	295(2)
μ, mm^{-1}	3.877	0.470	0.486
λ, Å	1.54178	0.71073	0.71073
data/restraints/ params	3242/0/323	3516/0/253	5591/0/326
solution method	direct methods	direct methods	direct methods
R, R_w (on F^2)	0.0350, 0.0914	0.0983, 0.2159	0.0587, 0.1615

[a] R_2 = Cl, R_3 = Ph. [b] Data from ref 21.

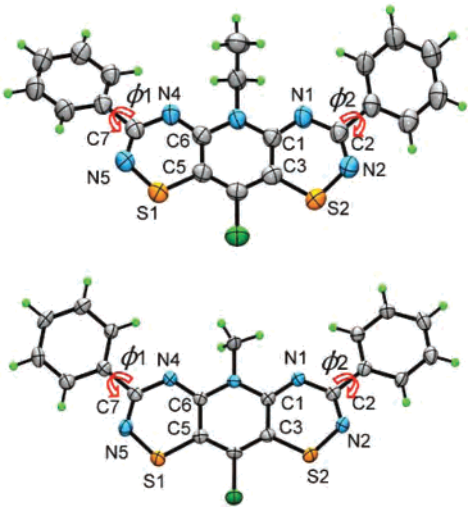

Figure 5. ORTEP drawings (50% thermal ellipsoids) of **7** (R_1 = Me, Et; R_2 = Cl, R_3 = Ph), with atom numbering. Torsion angles $\phi_{1,2}$ represent the average of two NCCC dihedral angles.

Table 3. Intramolecular Distances (Å) and Angles (deg)

	7 (R_1 = Et)[a]	**7** (R_1 = Me)[a,b]	[**7**][OTf] (R_1 = Me)[a,b]
S1−N5	1.6584(19)	1.657(5)	1.633(3)
S2−N2	1.663(2)	1.662(5)	1.612(3)
S1−C5	1.742(2)	1.726(5)	1.704(3)
S2−C3	1.739(2)	1.735(5)	1.690(3)
N4−C6	1.316(3)	1.318(6)	1.296(4)
N1−C1	1.327(3)	1.314(7)	1.301(3)
N4−C7	1.373(3)	1.372(6)	1.374(4)
N1−C2	1.370(3)	1.372(6)	1.365(4)
N5−C7	1.305(3)	1.304(7)	1.302(4)
N2−C2	1.301(3)	1.305(7)	1.317(4)
C5−C6	1.421(3)	1.427(7)	1.443(4)
C1−C3	1.417(3)	1.432(7)	1.436(4)
ϕ_1	12.3(3)	−2.1(1)	11.8(4)
ϕ_2	20.95(3)	−3.7(7)	−7.5(4)
δ	3.559(2)	3.436(4)	–
τ	38.74(1)	61.18(6)	–

[a] R_2 = Cl, R_3 = Ph; see text for definitions of *ϕ*, *δ*, and *τ*. [b] Data from ref 21.

Figure 5, and pertinent distances and angles are listed in Table 3. As a whole, the heterocyclic cores for both radicals are planar to within 0.042(4) Å for R_1 = Me and 0.42(2) Å for R_1 = Et. The torsion angles, $\phi_{1,2}$, for the two phenyl groups with respect to their respective thiadiazine rings

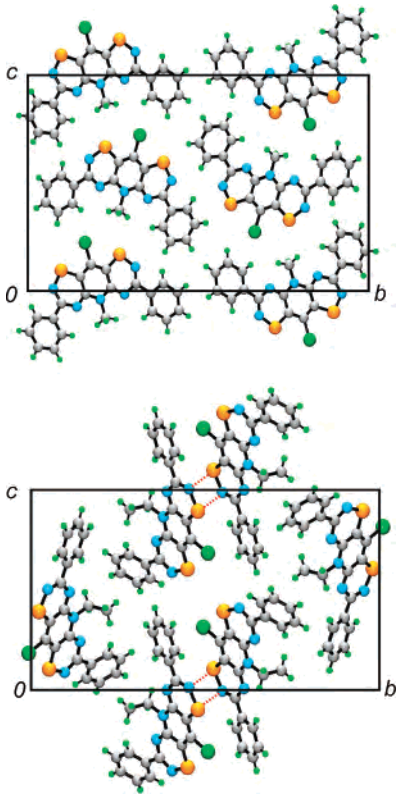

Figure 6. Unit cell drawings of **7** (R_2 = Cl, R_3 = Ph) for R_1 = Me (above) and R_1 = Et (below). Lateral intermolecular S1−N5′ contacts are shown with dashed lines.

indicate some twisting of the molecule for the ethyl derivative, but for R_1 = Me, the heterocycle and its ligands are close to being fully coplanar.

At a molecular level, the internal bond lengths and angles in the two radicals are remarkably similar, especially so given the different temperatures for data collection. There are, however, some changes in bond distances within the six-membered thiadiazine rings as a function of oxidation state (Table 3) that can be related to the bonding/antibonding properties of the a_2 SOMO (Figure 1). Occupation of this orbital upon reduction of the cation $\mathbf{7}^+$ to the radical **7** leads to a slight lengthening of the bonds to S1/S2 and N1/N4 and a concomitant shortening of the central C−C and C−N bonds. The effect is, however, smaller than that observed in monofunctional thiadiazinyls[20] and thiatriazinyls,[29] where the influence of the SOMO is concentrated on the bonds of a single six-membered ring.

Radicals **7** crystallize in the monoclinic space groups $P2_1/c$ (R_1 = Me) and $P2_1/n$ (R_1 = Et) with Z = 4. Figure 6 shows unit cell drawings of both radicals, from which it is apparent that the two phenyl groups on each radical serve as buffers that separate the heterocycles and reduce lateral intermolecular interactions. Indeed, for R_1 = Me, there are no S−S′ or S−N′ contacts inside or even close to the respective Van der Waals separations.[30] For R_1 = Et, the packing allows for the close lateral approach of two rings to afford a pair of

(29) Boeré, R. T.; Cordes, A. W.; Hayes, P. J.; Oakley, R. T.; Reed, R. W.; Pennington, W. T. *Inorg. Chem.* **1986**, *25*, 2445.
(30) Bondi, A. *J. Phys. Chem.* **1964**, *68*, 41.

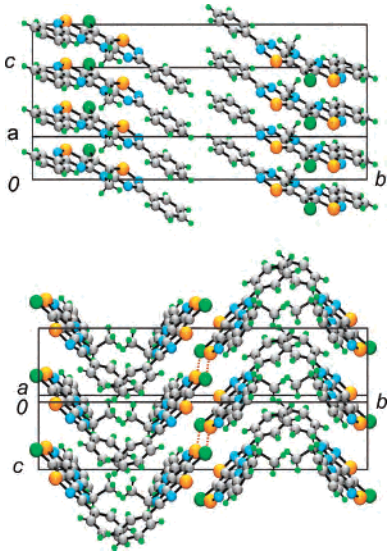

Figure 7. π-Stacked arrays **7** (R_2 = Cl, R_3 = Ph) for R_1 = Me (above) and R_1 = Et (below). Lateral intermolecular S1−N5′ contacts are shown with dashed lines.

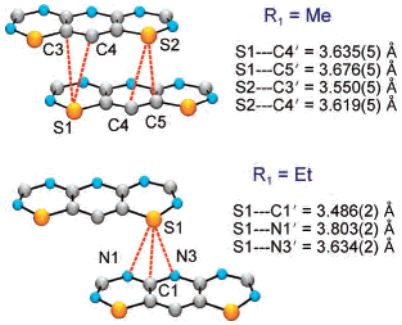

Figure 8. Intermolecular contacts within π-stacks of **7** (R_1 = Me, Et; R_2 = Cl, R_3 = Ph).

long (3.406(2) Å) S1−N5′ contacts, but otherwise, the radicals are well separated from one another in the *y* and *z* directions.

As illustrated in Figure 7, both radicals **7** (R_1 = Me, Et; R_2 = Cl, R_3 = Ph) form slipped π-stack arrays running along the *x* direction. The degree of slippage can be expressed in terms of τ (Table 3), the angle of inclination of the mean heterocyclic plane to the stacking axis. As will be shown below, the marked difference in τ angles for the two structures is the source of the differing electronic and magnetic properties of the two materials. The buffering effect of the phenyl groups, noted earlier, can also be clearly seen in these stacking diagrams. The only lateral intermolecular interactions are the S1−N5′ contacts found in the ethyl compound. Within the π-stacks, the plate-to-plate separation of neighboring heterocycles (δ in Table 3) is significantly smaller for the methyl derivative but, as demonstrated below, this closer spacing of the plates does not lead to enhanced electronic or magnetic interactions along the stacks. This can be appreciated upon inspection of the ring overlaps shown in Figure 8. In the methyl derivative, the closest interannular contacts involving sulfur are to carbon atoms C3, C4, and C5. One of these (C4) lies on a node in the SOMO, and the other two are outside the normal Van der Waals range. By contrast, in the ethyl derivative, plate slippage is so severe

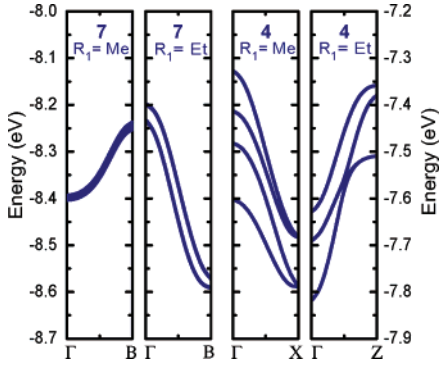

Figure 9. Crystal orbital dispersion in **7** (R_1 = Me, Et; R_2 = Cl, R_3 = Ph) and **4** (R_1 = Me, Et; R_2 = Cl).

that only a few close interannular contacts are possible. Only three involve sulfur atoms, but one of these (S1−C1′ = 3.486(2) Å) is aligned so as to afford a directly superimposed overlap of the $\rho\pi$-orbitals on sulfur and carbon. The role of this particular interaction on the electronic and magnetic structure of the ethyl radical is described below.

Band Structures. We have investigated the electronic structures of **7** (R_1 = Me, Et; R_2 = Cl, R_3 = Ph) by means of EHT band calculations. The results, displayed in the form of dispersion curves for the crystal orbitals (COs) arising from the four SOMOs in the unit cell, are shown in Figure 9. The dispersion plots are tracked from Γ (0, 0, 0) to B (1/2, 0, 0) of the reciprocal lattice, a direction which can be associated with orbital interactions along the stacking axis of the real space lattice. For purposes of comparison, analogous plots for the four SOMOs of bisdithiazolyls **4** (R_1 = Me, Et; R_2 = Cl)[15] are also shown, again monitored along the *k*-space vector that corresponds to the stacking direction in real space.

Within each class (**7** and **4**), the energies of the COs of the two radicals (with R_1 = Me, Et) flow in opposite directions as a function of *k* vector. For the methyl-subtituted bisdithiazolyls **4** (R_1 = Me), the energies of the four COs decrease with increase in *k* while those of the corresponding ethyl compound increase. These trends were earlier rationalized in terms of the overlap properties of the consecutive SOMOs along the slipped π-stacks; neighboring methyl radicals were associated with a *net* antibonding overlap at *k* = 0, while the ethyl radicals experienced a *net* bonding overlap.[15] The same argument applies to the present pair of radicals **7** (R_1 = Me, Et), although the resulting trend is the opposite of that seen in **4**. The relevant nearest-neighbor SOMO overlaps are illustrated in Figure 10. As may be seen, the sign of the overlaps arising from the close S−C′ contacts are positive (bonding) for R_1 = Me and negative (antibonding) for R_1 = Et. Moreover, on the basis of the length of the S−C′ contacts in the two compounds (Figure 8), the interactions along the stack should be far greater for the ethyl compound than for the methyl compound, a conclusion confirmed by the much larger dispersion of the COs for R_1 = Et. However, the most telling feature of the band structures of the two bisthiadiazinyls is the fact that the four COs of the methyl derivative are virtually coincident, an observation which reflects the fact that the four radicals in the unit cell

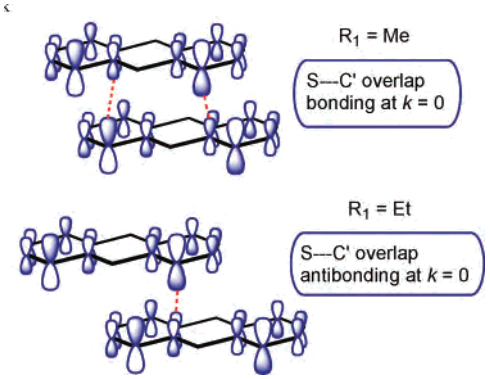

Figure 10. Sketches of nearest-neighbor SOMO overlaps in **7** (R_1 = Me, Et; R_2 = Cl, R_3 = Ph).

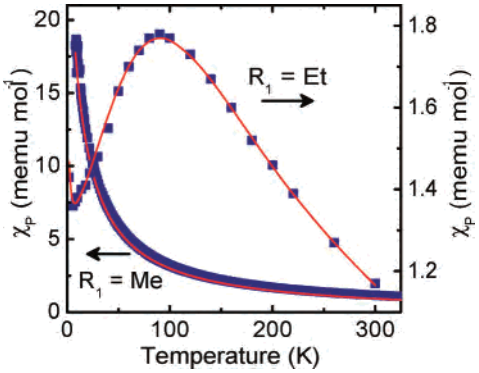

Figure 11. Magnetic susceptibility, χ_p, of **7** (R_1 = Me, Et; R_2 = Cl, R_3 = Ph) as a function of temperature. Data for R_1 = Me from ref 22.

are non-interacting, and that the material is essentially 1-D. The same conclusion can be reached for **7** (R_1 = Et), although here the pairwise lateral interactions (S1−N5′) lead to two closely spaced pairs of COs. This 1-dimensionality severely limits the overall bandwidth, *W*, of both radicals, although that of the ethyl compound reaches a value near 0.40 eV in spite of the restriction, but in neither case does *W* approach that seen for either of the two bisdithiazolyls **4**, where the four COs show considerable divergence as a result of lateral intermolecular S−S interactions. Indeed, the total band spreading of the two bisdithiazolyls can be ascribed as much to interstack effects as to intrastack overlap.

Transport Properties. The crystal and band structures of **7** (R_1 = Me, Et; R_2 = Cl, R_3 = Ph) underscore the importance of both strong inter- and intrastack radical−radical interactions in order to attain a high bandwidth. In the absence of both (R_1 = Me), or even just one (R_1 = Et) of these contributors, the electronic bandwidth, *W*, is insufficient of overcome the on-site Coulomb barrier, *U*, even though this parameter is projected to be relatively small for these systems. It is not surprising, therefore, that the pressed pellet[31] conductivity, σ(300 K), is less than 10^{-7} S cm^{-1} for both compounds.

While the 1-D nature of the electronic structures of both bisthiadiazinyls leads to limited charge transport, it also gives rise to some interesting magnetic effects. The results of variable-temperature magnetic susceptibility measurements on **7** (R_1 = Me, Et; R_2 = Cl, R_3 = Ph) are summarized in Figure 11, which shows plots of the paramagnetic susceptibility, χ_p, of the two compounds as a function of temperature. The pronounced maximum in χ_p near 90 K for the ethyl compound indicates the presence of significant antiferromagnetic (AFM) exchange coupling, while for the methyl derivative, no such maximum occurs above 2 K and a Curie−Weiss fit gives a Curie constant C = 0.360 emu K mol^{-1} and θ value of −11.9 K, suggesting the possibility of weak antiferromagnetic behavior. We have seen strong AFM coupling effects in earlier work on π-stacked bisdithiazolyls **4**,[17] but in those cases, the electronic interactions were numerous and the potential exchange pathways more complex, as a result of which it was not possible to model the magnetic data. Given the more 1-D nature of the electronic structure of **7** (R_1 = Et), with a single strong S1−C1′ interaction linking radicals along the π-stack and a much weaker lateral S1−N5′ interaction linking the stacks into pairs, we decided to model the temperature dependence of the χ_p data to a 1-D Heisenberg chain of AFM coupled S = 1/2 centers. On the basis of a Bonner−Fischer approach[32] and an $H_{ex} = -2\boldsymbol{J}\{S_1 \cdot S_2\}$ Hamiltonian, the derived fit (shown in Figure 11) was obtained using the following parameters: $\boldsymbol{J}$ = −49 cm^{-1}, $z\boldsymbol{J}$ = −3 cm^{-1}, g = 2.007, θ = 0 cm^{-1}, α = 0.001, TIP = 2.2 × 10^{-4} emu mol^{-1}, and $R(\chi)$ = 0.0157.[33] The exchange equation was modified to include a molecular field correction, which suggested a small long-range AFM component.

In order to explore the origins of the magnetic properties of the two bisthiadiazinyls, we have performed a series of DFT calculations in an attempt to characterize the individual exchange interactions involved. We have used broken symmetry methods[34] to estimate the singlet−triplet exchange energies for closely interacting radical pairs, an approach which has been successfully applied to a variety of nitrogen-centered radicals[35] and, more recently, to heterocyclic thiazyl radicals.[36,37] Accordingly, and with reference to the Hamiltonian $H_{ex} = -2\boldsymbol{J}\{S_1 \cdot S_2\}$, the exchange energy, J, for any pair of interacting radicals can be estimated from the total energies of the triplet (E_{TS}) and broken symmetry singlet (E_{BSS}) states and the respective expectation values $<S^2>$ of the two states, according to eq 1.

$$J = \frac{-(E_{TS} - E_{BSS})}{<S^2>_{TS} - <S^2>_{BSS}} \qquad (1)$$

Exchange energies were calculated with a simple dinuclear nearest-neighbor exchange model using a variety of pairwise

(31) Wudl, F.; Bryce, M. R. *J. Chem. Educ.* **1990**, *67*, 714.

(32) Bonner, J. C.; Fischer, M. E. *Phys. Rev.* **1964**, *135*, A640.

(33) $R(\chi) = [E(\chi_{obs}-\chi_{calc})^2/E(\chi_{obs})^2]^{1/2}$, α = fraction of monomeric paramagnetic impurity, TIP = temperature independent paramagnetism.

(34) (a) Noodleman, L.; Norman, J. G. *J. Chem. Phys.* **1979**, *70*, 4903. (b) Noodleman, L. *J. Chem. Phys.***1981**, *74*, 5737.

(35) (a) Novoa, J. J.; Deumal, M. *Struct. Bonding* **2001**, *100*, 33. (b) Jornet, J.; Deumal, M.; Ribas-Ariño, J.; Bearpark, M. J.; Robb, M. A.; Hicks, R. G.; Novoa, J. J. *Chem. Eur. J.* **2006**, *12*, 3995.

(36) (a) Rawson, J. M.; Luzon, J.; Palacio, F. *Coord. Chem. Rev.* **2005**, *249*, 2631. (b) Luzon, J.; Campo, J.; Palacio, F.; McIntyre, G. J.; Rawson, J. M. *Polyhedron* **2005**, *24*, 2579.

(37) Decken, A.; Mattar, S. M.; Passmore, J.; Shuvaev, K. V.; Thompson, L. K. *Inorg. Chem.* **2006**, *45*, 3878.

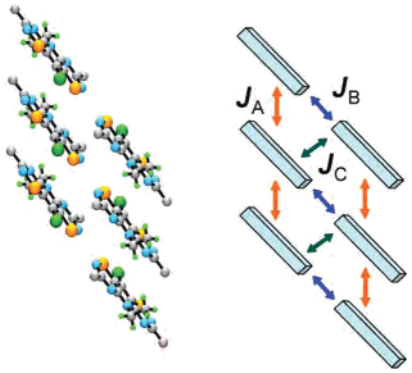

Figure 12. Magnetic exchange pathways J_A, J_B, and J_C in **7** (R_1 = Et, R_2 = Cl, R_3 = Ph).

Table 4. Calculated Exchange Coupling Constants[a]

	6-31G(d,p)	6-311G(d,p)	6-311+G(d,p)
7 (R_1 = Me)			
J_A	−14.4	−9.3	−7.5
7 (R_1 = Et)			
J_A	−32.2	−32.7	−32.9
J_B	−5.6	−7.8	−8.5
J_C	−3.5	−4.3	−4.6

[a] J values (cm^{-1}) in **7** (R_1 = Me, Et; R_2 = Cl, R_3 = Ph) calculated from eq 1 using single-point B3LYP electronic energies. J_A, J_B, and J_C for R_1 = Et are defined in Figure 12.

combinations of radicals, with atomic coordinates taken from crystallographic data. For the methyl-substituted compound, only one possible exchange pathway, J_A, was considered, namely that involving the interaction of nearest-neighbor radicals along the π-stack. For the ethyl derivative, the lateral interactions noted above give rise to a ladderlike structure (Figure 12) in which there are three possible exchange couplings, J_A, J_B, and J_C. As in the methyl compound, the J_A pathway involves radical−radical interactions along the π-stacks while J_B is associated with the lateral S1−N5′ contacts noted above. The potential third coupling J_C arises from the head-over-tail pairing of radicals in adjacent π-stacks. Single-point total energies were calculated using the hybrid exchange correlation functional B3LYP and a series of polarized, split-valence basis sets with double-ζ (6-31G(d,p)), triple-ζ (6-311G(d,p)), and triple-ζ plus diffuse (6-311+G(d,p)) functions.

The results are summarized in Table 4, which shows individual exchange energies as a function of basis set. Overall, there is fair consistency across the basis sets, certainly sufficient for a qualitative evaluation of the relative importance of the various pathways. In both cases (R_1 = Me, Et), the calculations predict an antiferromagnetic exchange interaction, J_A, along the stacking axis, that of the ethyl compound being substantially larger, as anticipated from the structural features noted above. Within a mean field model, the 6-311+G(d,p) J_A exchange energy for R_1 = Me translates (with two equivalent neighbors) into a predicted Curie−Weiss θ value of −23.6 K, a value higher than that observed experimentally, but not overly so. There are similar discrepancies between the 6-311+G(d,p) J_A and $J_{B,C}$ energies and those derived from the 1-D Heisenberg chain model with the molecular field term included, but given the size of the radicals, the correspondence between DFT calculations and the modified chain model is reasonable.

Summary. The development of single-component neutral radical conductors is based on the need to design thermally stable radicals with a low on-site Coulomb repulsion energy, U, and a high bandwidth, W. In recent years, we have explored the use of resonance stabilization of heterocyclic thiazyl and selenazyl radicals to lower the value of U. The two bisthiadiazinyls **7** (R_1 = Me, Et; R_2 = Cl, R_3 = Ph) described here represent the first examples of a new family of such compounds. Their low electrochemical cell potentials and highly delocalized spin distributions match those of the more extensively studied bisdithiazolyls **4** and, as such, represent the closest approach yet to a heterocyclic radical that fulfills the low U criterion. Moreover, bisthiadiazinyls are far more thermally stable than bisdithiazolyls, and the presence of the R_3 ligand provides flexibility for further electronic modification. The two radicals described here do not dimerize in the solid state but form evenly spaced slipped π-stack arrays. The unpaired electrons associated with the radicals are not, however, charge carriers; instead, the ambient temperature conductivity is well below 10^{-7} S cm^{-1}. This lack of conductivity of **7** relative to **4** is, we believe, the direct result of a loss in bandwidth, W, occasioned by the steric bulk of the phenyl groups in the R_3 positions. Their presence reduces intrastack contacts and, more importantly, all but eliminates lateral interstack interactions. Consistently, the EHT calculations indicate weak and highly 1-D band electronic structures, especially for R_1 = Me. While the relative isolation of the radicals reduces conductivity, it also leads to a simplification of their magnetic structures. The weak AFM coupling observed for R_1 = Me and stronger AFM coupling found for R_1 = Et are consistent with 1-D chains of weakly coupled $S = {}^1/_2$ units, and the magnitude of the exchange couplings in both compounds has been modeled by broken symmetry DFT methods. Future work will focus on the design of smaller ligands in the R_3 position, to increase W, and the use of electron releasing and withdrawing groups, to decrease U. Selenium incorporation,[38] an approach which has afforded dramatic increases in the conductivity of bisdithiazolyls **4**,[18] is also being pursued.

Experimental Section

General Procedures and Starting Materials. The reagents 2,6-diaminopyridine, aluminum trichloride, benzonitrile, sodium carbonate monohydrate, thionyl chloride, nitrosonium hexafluoroantiminonate, Proton-Sponge, dimethylferrocene (DiMFc), and methyl and ethyl trifluoromethanesulfonate were obtained commercially. All were used as received, save for DiMFc, which was sublimed and recrystallized from acetontrile before use. All solvents were of at least reagent grade; acetonitrile (MeCN) and dichloroethane (DCE) were dried by distillation from P_2O_5. All reactions were performed under an atmosphere of dry nitrogen. Melting points are uncorrected. Fractional sublimations were performed in an ATS series 3210 three-zone tube furnace, mounted horizontally, and linked to a series 1400 temperature-control system. Infrared spectra

(38) Kloc, K.; Mlochowski, J.; Osajda, K.; Syper, L.; Wojtowicz, H. *Tetrahedron Lett.* **2002**, *43*, 4071.

(Nujol mulls, KBr optics) were recorded on a Nicolet Avatar FTIR spectrometer (at 2 cm^{-1} resolution), and visible spectra were collected using a Beckman DU 640 spectrophotometer. ^1H NMR spectra were run on a Bruker Avance 300 MHz NMR spectrometer. Fluorescence spectra were recorded on a PTI Quantamaster QM-2 fluorimeter. Low-resolution mass spectra (70 eV, EI, DEI and CI, DCI) were run on a Micromass Q-TOF Ultima Global LC/MS/MS system or a JEOL HX110 double-focusing mass spectrometer. Elemental analyses were performed by MHW Laboratories, Phoenix, AZ.

Preparation of *N*′,*N*″-Pyridine-2,6-diyldibenzenecarboximidamide (8). Aluminum chloride (12.2 g, 0.0916 mol), benzonitrile (9.50 mL, 0.0921 mol), and 2,6-diaminopyridine (5.00 g, 0.0458 mol) were combined and melted together at 200 °C for 15 min. The hard glassy solid was heated into 50 mL of 10% aqueous HCl solution, which turned over to a brown crystalline solid that was filtered and washed with 20 mL 20% aqueous HCl solution. This hydrochloride salt (14.5 g, 0.0412 mol) was dissolved in 100 mL of boiling water and, on cooling, 100 mL of aqueous sodium carbonate monohydrate solution (35.3 g, 0.284 mol) was added to afford a light brown solid, which was filtered off and washed with water. The bis-amidine **8** was recrystallized from MeCN as light brown flakes, yield 9.48 g (0.0301 mol, 73%); mp 177.5−180.5 °C. IR: 3421 (m), 3274 (m), 1622 (s), 1584 (s), 1527 (s), 1492 (m), 1432 (w), 1320 (m), 1244 (m), 1182 (w), 1153 (m), 1078 (w),1028 (m), 969 (w), 826 (m), 795 (m), 787 (m), 698 (s), 522 (w), 485 (w) cm^{-1}. ^1H NMR (CD_3CN): 7.97 (m, 2H), 7.68 (t, 1H, J = 7.7 Hz), 7.49 (m, 3H), 6.76 ppm (d, 2H, J = 7.7 Hz). Anal. Calcd for $C_{19}H_{17}N_5$: C, 72.36; H, 5.43; N, 22.21%. Found: C, 72.21; H, 5.61; N, 21.99%.

Preparation of 10-Chloro-3,7-diphenyl-5*H*-[1,2,4]thiadiazino-[6′,5′:5,6]pyrido[2,3-*e*][1,2,4]-thiadiazin-1-ium Hexafluoroantimonate ([7][SbF_6], R_1 = H, R_2 = Cl, R_3 = Ph). Sulfur monochloride (10.1 g, 0.0747 mol) was added to a slurry of **8** (3.92 g, 0.0124 mol) in 125 mL of chlorobenzene. The reaction mixture was set to reflux for 16 h, and the resulting precipitate was collected by filtration and washed with 2 × 60 mL of chlorobenzene. Crude [**7**][Cl] (R_1 = H, R_2 = Cl, R_3 = Ph) was obtained as a green-brown powder, yield 5.09 g (0.0114 mol, 93%). IR: 1885 (m), 1631 (w), 1596 (w), 1583 (w), 1556 (w), 1362 (s), 1233 (s), 1176 (w), 1043 (m), 1073 (m), 1064 (m), 1027 (m), 1000 (w), 972 (w), 845 (w), 829 (w), 775 (s), 789 (m), 696 (s), 664 (m), 624 (w), 585 (m), 535 (w), 472 (m), 453 (w) cm^{-1}. A sample of [**7**][Cl] (R_1 = H, R_2 = Cl, R_3 = Ph) (5.09 g, 0.0114 mol) was added to a colorless solution of nitrosonium hexafluoroantimonate (3.67 g, 0.0138 mol) in 70 mL of MeCN to give a dark blue solution with lustrous red precipitate. After 1 h, the solvent was removed by flash distillation and the residue was filtered using 60 mL of HOAc. The product, [**7**][SbF_6] (R_1 = H, R_2 = Cl, R_3 = Ph), was washed with 2 × 50 mL of HOAc to afford a dark green crystalline solid, yield 4.03 g (0.00633 mol, 55%); dec 255 °C. IR: 3224 (w), 1586 (m), 1561 (m), 1531 (m), 1407 (w), 1322 (s), 1237 (s), 1178 (m), 1149 (w), 1073 (w), 1061 (s), 1027 (m), 1000 (w), 938 (w), 821 (w), 788 (w), 774 (s), 725 (w), 695 (s), 664 (s), 652 (s), 643 (m), 581 (s), 564 (w), 460 (w) cm^{-1}. ^1H NMR (CD_3CN): 7.65 (m, 3H), 8.20 ppm (m, 2H). Anal. Calcd for $C_{19}H_{11}ClF_6N_5S_2Sb$: C, 35.40; H, 1.72; N, 10.86%. Found: C, 35.41; H, 2.00; N, 10.63%.

Preparation of 10-Chloro-3,7-diphenyl[1,2,4]thiadiazino[6′,5′:5,6]pyrido[2,3-*e*][1,2,4]thiadiazin-1-ium-5-ide (9, R_2 = Cl, R_3 = Ph). Proton-Sponge (1.61 g, 7.54 mmol) was added to a slurry of [**7**][SbF_6] (R_1 = H, R_2 = Cl, R_3 = Ph) (4.01 g, 3.21 mmol) in 125 mL of MeCN to give a purple precipitate of **9** (R_2 = Cl, R_3 = Ph) that was collected by filtration and washed with 2 × 50 mL of MeCN, yield 2.28 g (5.59 mmol, 90%); mp >320 °C. IR: 1627 (w), 1584 (w), 1507 (w), 1489 (w), 1432 (s), 1410 (w), 1343 (w), 1313 (m), 1302 (m), 1179 (s), 1070 (w), 1053 (w), 1028 (m), 9321 (w), 866 (w), 847 (w), 779 (s), 764 (s), 722 (w), 708 (s), 693 (w), 627 (s), 597 (m), 553 (w), cm^{-1}. Anal. Calcd for $C_{19}H_{10}ClN_5S_2$: C, 55.95; H, 2.47; N, 17.17%. Found: C, 55.81; H, 2.25; N, 17.36%.

Preparation of 10-Chloro-5-methyl-3,7-diphenyl-5*H*-[1,2,4]-thiadiazino[6′,5′:5,6]pyrido[2,3-*e*][1,2,4]thiadiazin-1-ium Trifluoromethanesulfonate ([7][OTf], R_1 = Me, R_2 = Cl, R_3 = Ph). Methyl trifluoromethanesulfonate (0.340 mL, 3.00 mmol) was added to a slurry of **9** (R_2 = Cl, R_3 = Ph) (1.00 g, 2.45 mmol) in 8 mL of DCE to give a turquoise slurry that was stirred for 16 h. The brown precipitate of [**7**][OTf] (R_1 = Me, R_2 = Cl, R_3 = Ph) was filtered off and washed with 2 × 10 mL of DCE. The crude product was recrystallized in MeCN to afford a mixture of red rhombohedral plates and needles, yield 0.970 g (1.70 mmol, 69%); dec 248 °C for rhombohedral plates. IR of rhombohedral plates: 1583 (w), 1530 (m), 1335 (s), 1314 (w), 1272 (m), 1263 (s), 1223 (w), 1158 (m), 1136 (m), 1039 (w), 1030 (m), 1022 (w), 966 (m), 838 (w), 809 (w), 794 (w), 775 (s), 750 (m), 722 (w), 722 (s), 701 (m), 692 (m), 680 (s), 636 (w), 621 (w), 573 (w), 559 (w), 520 (w), 498 (w) cm^{-1}. IR for needles: 1583 (m), 1530 (m), 1414 (s), 1337 (s), 1312 (w), 1264 (s), 1223 (w), 1179 (w), 1148 (s), 1097 (w), 1032 (s), 1023 (s), 966 (m), 840 (w), 814 (w), 779 (s), 749 (s), 697 (s), 680 (m), 637 (s), 621 (m), 573 (w), 559 (w), 517 (m), 500 (w) cm^{-1}. ^1H NMR of rhombohedral plates (CD_3CN): 3.90 (s, 3H, C*H*$_3$), 7.64 (m, 3H), 8.26 ppm (m, 2H). UV−vis: λ_{max} 622 nm, log ϵ 4.7. Anal. Calcd for rhombohedral plates, $C_{21}H_{13}ClF_3N_5O_3S_3$: C, 44.09; H, 2.29; N, 12.24%. Found: C, 44.25; H, 2.40; N, 11.99%.

Preparation of 10-Chloro-5-ethyl-3,7-diphenyl-5*H*-[1,2,4]thiadiazino[6′,5′:5,6]pyrido[2,3-*e*][1,2,4]-thiadiazin-1-ium Trifluoromethanesulfonate ([7][OTf], R_1 = Et, R_2 = Cl, R_3 = Ph). A slurry of **9** (R_2 = Cl, R_3 = Ph) (1.00 g, 2.45 mmol) and ethyl trifluoromethanesulfonate (0.380 mL, 2.93 mmol) in 8 mL of DCE was stirred for 32 h. The brown precipitate of [**7**][OTf] (R_1 = Et, R_2 = Cl, R_3 = Ph) was filtered off and washed with 2 × 10 mL of DCE. The crude product was recrystallized from MeCN as bronze needles, yield 0.638 g (1.09 mmol, 45%); dec 278 °C. IR: 1595 (w), 1582 (m), 1529 (m), 1337 (s), 1263 (s), 1234 (w), 1176 (w), 1145 (s), 1111 (w), 1069 (s), 1048 (s), 1031 (s), 932 (w), 787 (m), 774 (s), 753 (s), 698 (s), 678 (m), 636 (s), 619 (m), 571 (m), 517 (m) cm^{-1}. ^1H NMR (CD_3CN): 1.45 (t, 3H, CH_2CH_3, J = 7.0 Hz), 4.67 (m, 2H, CH_2CH_3, J = 7.0 Hz), 7.65 (m, 3H), 8.26 ppm (m, 2H). UV−vis: λ_{max} 619 nm, log ϵ 4.8. Anal. Calcd for $C_{22}H_{15}ClF_3N_5O_3S_3$: C, 45.09; H, 2.58; N, 11.95%. Found: C, 45.17; H, 2.43; N, 11.99%.

Preparation of 10-Chloro-5-methyl-3,7-diphenyl-2*H*,5*H*-[1,2,4]thiadiazino-[6′,5′:5,6]pyrido[2,3-*e*][1,2,4]thiadiazin-2-yl (7, R_1 = Me, R_2 = Cl, R_3 = Ph). Dimethylferrocene (0.443 g, 2.07 mmol) was added to a solution of [**7**][OTf] (R_1 = Me, R_2 = Cl, R_3 = Ph) (0.970 g,1.70 mmol) in 100 mL of degassed MeCN. The maroon microcrystalline material was filtered after 1 h and washed with 2 × 50 mL of MeCN, yield 0.630 g (1.49 mmol, 88%); mp 228−230 °C. IR: 1583 (m), 1536 (s), 1500 (m), 1444 (s), 1403 (w), 1336 (w), 1308 (s), 1277 (s), 1246 (w), 1177 (s), 1116 (w), 1069 (w), 1030 (s), 1018 (w), 1000 (m), 953 (m), 921 (m), 852 (w), 785 (m), 760 (s), 728 (s), 693 (s), 677 (m), 672 (m), 621 (m), 616 (m), 543 (w), 486 (w), 451 (w) cm^{-1}. Anal. Calcd for $C_{20}H_{13}ClN_5S_2$: C, 56.80; H, 3.10; N, 16.56%. Found: C, 56.68; H, 3.30; N, 16.38%. Crystals suitable for structure analysis were grown by vacuum sublimation at 10^{-4} Torr down a temperature gradient of 210−100 °C.

Preparation of 10-Chloro-5-methyl-3,7-diphenyl-2*H*,5*H*-[1,2,4]-thiadiazino-[6′,5′:5,6]pyrido[2,3-*e*][1,2,4]thiadiazin-2-yl (7, R_1 = Et, R_2 = Cl, R_3 = Ph). Dimethylferrocene (0.230 g, 1.07 mmol) was added to a degassed solution of [**7**][OTf] (R_1 = Et, R_2 = Cl, R_3 = Ph) (0.513 g, 0.088 mmol) in 40 mL of MeCN. After 30 min, the maroon microcrystalline material was filtered off and washed with 2 × 30 mL of MeCN, yield 0.323 g (0.739 mmol, 84%); dec >200 °C. IR: 1583 (w), 1545 (m), 1521 (w), 1499 (s), 1347 (w), 1312 (s), 1299 (w), 1277 (s), 1219 (m), 1181 (m), 1090 (w), 1037 (m), 1023 (s), 993 (s), 931 (w), 920 (w), 780 (m), 755 (s), 736 (s), 705 (w), 695 (s), 691 (s), 678 (w), 667 (m), 616 (m), 559 (w), 484 (w) cm^{-1}. Anal. Calcd for $C_{21}H_{15}ClN_5S_2$: C, 57.72; H, 3.46; N, 16.03%. Found: C, 58.12; H, 3.62; N, 16.24%. Crystals suitable for X-ray work were grown by vacuum sublimation at 10^{-4} Torr down a temperature gradient of 200−100 °C.

X-ray Measurements. A needle of **7** (R_1 = Et, R_2 = Cl, R_3 = Ph) was glued to a glass fiber with epoxy. X-ray data were collected at 298 K on a Bruker SMART APEX CCD-based diffractometer using T-scans. The reflection data were processed using SAINT,[39] and the structure was solved by direct methods using SHELXS-90[40] and refined by least-squares methods on F^2 using SHELXL-97[41] incorporated in the SHELXTL[42] suite of programs. All non-hydrogen atoms were refined anisotropically; hydrogen atoms were located on difference maps and refined isotropically. Details of data collection and refinement are presented in Table 2.

Magnetic Susceptibility Measurements. Variable-temperature magnetic susceptibility measurements on **7** (R_1 = Et, R_2 = Cl, R_3 = Ph) were performed on a Quantum Design MPMS5S SQUID magnetometer operating at 0.1 T. Diamagnetic corrections were made using Pascal's constants,[43] and the data were modeled using a standard Heisenberg 1-D chain fit function.[44] The magnetic data on **7** (R_1 = Me, R_2 = Cl, R_3 = Ph) are as reported in ref 21 and were measured on a George Associates Faraday balance operating at 0.1 T.

EPR Spectra. X-Band EPR spectra were recorded at ambient temperature using a Bruker EMX-200 spectrometer; samples of the radicals were dissolved in degassed dichloromethane. Hyperfine coupling constants were obtained by spectral simulation using Simfonia[45] and WinSim.

Cyclic Voltammetry. Cyclic voltammetry was performed using a PINE Bipotentiostat, model AFCClBP1, with scan rates of 50−100 mV s^{-1} on solutions (<10^{-3} M) of [**7**][OTf] (R_1 = Me, Et; R_2 = Cl, R_3 = Ph) in CH_3CN (dried by distillation from P_2O_5 and CaH_2) containing 0.1 M tetra-*n*-butylammonium hexafluorophosphate as supporting electrolyte. Potentials were scanned with respect to the quasi-reference electrode in a single compartment cell fitted with Pt electrodes and referenced to the Fc/Fc^+ couple of ferrocene at 0.38 V vs SCE.[46] The $E_{pa}-E_{pc}$ separations of the reversible couples were within 10% of that of the Fc/Fc^+ couple.

DFT Calculations. The calculated ion energetics (IP, EA, and ΔH_{disp}) and spin density data for **7** (R_1 = R_2 = R_3 = H) shown in Figure 2 were estimated by using the B3LYP method, as contained in the Gaussian 03 suite of programs.[47] Adiabatic (ΔSCF) ionization potential and electron affinity estimates were obtained from total electronic energy calculations using a 6-31G(d,p) basis set within the constraints of C_{2v} symmetry. Frequency calculations on all states confirmed that they were stationary points. Exchange energies for interacting radicals (with all ligands included) were computed from eq 1, using single-point B3LYP energies of the lowest triplet and broken symmetry singlet states and their respective $<S^2>$ expectation values. Tight convergence criteria (RMSDP = 10^{-8}) were employed for all basis sets save 6-311+G(d,p), where convergence was set at RMSDP = 10^{-7}. Atomic coordinates were taken from crystallographic data.

Band Calculations. Band electronic structure calculations were performed with the EHMACC suite of programs[48] using the Coulomb parameters of Baasch, Viste, and Gray[49] and a quasi-split valence basis set adapted from Clementi and Roetti;[50] numerical values are tabulated elsewhere.[51] The off-diagonal elements of the Hamiltonian matrix were calculated with the standard weighting formula.[52] Atomic positions were taken from the crystallographic data.

Acknowledgment. We thank the Natural Sciences and Engineering Research Council of Canada (NSERCC) for financial support. We also acknowledge the Canada Council for the Arts for a Killam Research Fellowship to R.T.O. and the NSERCC for a post-graduate scholarship to A.A.L.

Supporting Information Available: Details of DFT calculations and of X-ray crystallographic data collection and structure refinement, including tables of atomic coordinates, bond distances and angles, anisotropic thermal parameters, and hydrogen atom positions in CIF format. This material is available free of charge via the Internet at http://pubs.acs.org.

IC0700405

(39) *SAINT, version 6.22*; Bruker Advanced X-ray Solutions, Inc.: Madison, WI, 2001.
(40) Sheldrick, G. M. SHELXS-90. *Acta Crystallogr. A* **1990**, *46*, 467.
(41) Sheldrick, G. M. *SHELXL-97, Program for the Refinement of Crystal Structures*; University of Göttingen: Göttingen, Germany, 1997.
(42) *SHELXTL, VERSION 6.12, Program Library for Structure Solution and Molecular Graphics*; Bruker Advanced X-ray Solutions, Inc.: Madison, WI, 2001.
(43) Carlin, R. L. *Magnetochemistry*; Springer-Verlag: New York, 1986.
(44) Estes, W. E.; Gavel, D. P.; Hatfield, W. E.; Hodgson, D. J. *Inorg. Chem.* **1978**, *17*, 1415.
(45) *WinEPR Simfonia, version 1.25*; Bruker Instruments, Inc.: Billerica, MA, 1966.
(46) Boeré, R. T.; Moock, K. H.; Parvez, M. *Z. Anorg. Allg. Chem.* **1994**, *620*, 1589.
(47) Frisch, M. J.; Trucks, G. W.; Schlegel, H. B.; Scuseria, G. E.; Robb, M. A.; Cheeseman, J. R.; Montgomery, J. A., Jr.; Vreven, T.; Kudin, K. N.; Burant, J. C.; Millam, J. M.; Iyengar, S. S.; Tomasi, J.; Barone, V.; Mennucci, B.; Cossi, M.; Scalmani, G.; Rega, N.; Petersson, G. A.; Nakatsuji, H.; Hada, M.; Ehara, M.; Toyota, K.; Fukuda, R.; Hasegawa, J.; Ishida, M.; Nakajima, T.; Honda, Y.; Kitao, O.; Nakai, H.; Klene, M.; Li, X.; Knox, J. E.; Hratchian, H. P.; Cross, J. B.; Bakken, V.; Adamo, C.; Jaramillo, J.; Gomperts, R.; Stratmann, R. E.; Yazyev, O.; Austin, A. J.; Cammi, R.; Pomelli, C.; Ochterski, J. W.; Ayala, P. Y.; Morokuma, K.; Voth, G. A.; Salvador, P.; Dannenberg, J. J.; Zakrzewski, V. G.; Dapprich, S.; Daniels, A. D.; Strain, M. C.; Farkas, O.; Malick, D. K.; Rabuck, A. D.; Raghavachari, K.; Foresman, J. B.; Ortiz, J. V.; Cui, Q.; Baboul, A. G.; Clifford, S.; Cioslowski, J.; Stefanov, B. B.; Liu, G.; Liashenko, A.; Piskorz, P.; Komaromi, I.; Martin, R. L.; Fox, D. J.; Keith, T.; Al-Laham, M. A.; Peng, C. Y.; Nanayakkara, A.; Challacombe, M.; Gill, P. M. W.; Johnson, B.; Chen, W.; Wong, M. W.; Gonzalez, C.; Pople, J. A. *Gaussian 03*, revision C.02; Gaussian, Inc.: Wallingford, CT, 2004.
(48) EHMACC, Quantum Chemistry Program Exchange, program number 571.
(49) Basch, H.; Viste, A.; Gray, H. B. *Theor. Chim. Acta* **1965**, *3*, 458.
(50) Clementi, E.; Roetti, C. *At. Data Nucl. Data Tables* **1974**, *14*, 177.
(51) Cordes, A. W.; Haddon, R. C.; Oakley, R. T.; Schneemeyer, L. F.; Waszczak, J. V.; Young, K. M.; Zimmerman, N. M. *J. Am. Chem. Soc.* **1991**, *113*, 582.
(52) Ammeter, J. H.; Bürgi, H. B.; Thibeault, J. C.; Hoffmann, R. *J. Am. Chem. Soc.* **1978**, *100*, 3686.